Defining a generic accelerated erosion testing method for earthen materials

Christopher Beckett[1*] and *Paulina* Faria[2]

[1]Institute for Infrastructure and Environment, School of Engineering, The University of Edinburgh, Scotland
[2]CERIS, Department of Civil Engineering, NOVA School of Science and Technology, NOVA University Lisbon, Portugal

Abstract. The 1952 CSIRO accelerated erosion test was the first to appraise the quality and potential longevity of earthen construction materials. The test measures the depth of erosion resulting from a spray of water delivered at a set pressure and distance from a nozzle of controlled geometry. The test has remained popular, due to its simplicity, and forms the basis of the design for durability in the current New Zealand earthen construction standards (and their derivatives). However, it is now recognised that the accelerated erosion test does not capture the full range of exposure conditions likely to affect an earthen structure during its lifetime. As such, academics and practitioners have suggested variations to the test, to reproduce erosion which is observed in the field. However, this makes it difficult to compare the results of one test to another, and so prevents any standardised material assessment. As earthen construction materials grow in interest in the unsaturated soils community, it is becoming necessary to understand and explore the limitations of these materials beyond their hydromechanical properties and to compare results between investigations fairly. This paper presents the concept of a 'generic' accelerated erosion test method and examines the effect of the spray pressure and spray distance on the erosive force delivered to the test specimen, to understand how these variables could be normalised. The generic method, when developed, will remove the strict restrictions of the original apparatus, making the test universally accessible.

1 Introduction

Earthen building materials are becoming a popular topic of study within the unsaturated soils community. Earthen materials are those that use soil as the sole or primary material to create construction elements. The soil can be used 'raw' or combined with cementitious or non-cementitious binders (cement, lime, bitumen, biopolymers) to improve its mechanical properties and/or its resistance to water. Even without stabilisers, however, the most competent earthen materials can boast unconfined compressive strengths above 1 MPa. The role of suction in achieving these high strengths is well known (e.g. [1]) and, given their exposure to the atmosphere on all sides, suction in earthen materials can exceed 100 MPa whilst degrees of saturation dip below 5%. These conditions are beyond the residual suction range, i.e. where slight changes in degree of saturation can create changes in suction of orders of magnitude, with an associated variation in the mechanical properties of c. 50% from the most to the least favourable cases [2]. Understanding and controlling the role of suction in these materials is therefore paramount, as is protecting them and preventing them from absorbing water.

The sensitivity to water of earthen materials dominated heritage design practices and remains the greatest barrier to their wider adoption in industry [3]. The first attempt to characterise an earthen material's susceptibility to water, referred to hereafter as its "durability", was the Commonwealth Scientific and Industrial Research Organisation (CSIRO) Accelerated Erosion Test (AET) [4]. The test comprises spraying a specimen with water at a controlled pressure for a specified duration. The test was developed in response to an emerging interest in using earth for construction in Australia but for an industry that, apart from the early pioneers, had no experience or confidence in its use. The AET as specified in 1952 is still referred to in the New Zealand Standards 4297/4298/4299 [5-7] (upon which United States ASTM E2392 [8] also depends) to determine a material's "erodibility index" [6], from which a designer can determine an element's acceptable degree of exposure (e.g. it may compose a wall that can be exposed to rain, that is partially defended, or must be completely defended by an overhanging roof).

Various studies have, over the past decades, demonstrated that the AET does not reflect the natural protracted degradation of earthen elements [9]. Researchers and practitioners have therefore suggested variations to the AET in terms of different delivery pressures, spray distances, spray times, and/or nozzle configurations to try to improve the match to observed decay (e.g. [10]). Similarly, some have used alternative components (e.g. nozzle types) to those originally specified as the required components are either expensive or not available (consider that earthen construction is used in many poorer countries where certain equipment cannot be accessed). Such

* Corresponding author: christopher.beckett@ed.ac.uk

modifications permit testing where otherwise it might be avoided and improve its match to local conditions but mean that it is difficult to contrast one test result against another. A method to harmonize AET testing, which can accept and accommodate these local modifications, would allow practitioners and designers greater flexibility when adopting earthen materials whilst facilitating a comparison back to the 'standard' procedure required by NZS 4298 [6].

This paper explores how a generic framework to compare variations of the AET to each other might be constructed. The study examines the force delivered to the target by a water spray for different separation distances and delivery pressures, to compare those results to theoretical forces from hydraulic theory. We use the results to understand the bounds on a successful framework and how reliable such a framework could be when considering real variations in experimental procedures and accuracy. This work was originally part of Standards Australia committee BD 083 to update durability testing methods specified within the Standards Australia HB 195 *Australian Earth Building* handbook [11] and contributes to work being carried out under the RILEM Technical Committee MAE *Mechanical Performance and Durability Assessment of Earthen Elements and Structures*.

2 Experimental programme

2.1 The CSIRO accelerated erosion test

The CSIRO AET comprises a water spray, fired at a pressure of 50 kPa from a specified nozzle geometry at an exposed area of earthen element, placed 470 mm from the nozzle exit, as shown in Figure 1 [6]. The separation distance ensures that the spray strikes the specimen across an approximately circular area of 150 mm diameter. The specimen is sprayed for one hour and the depth of erosion is tested at ten-minute intervals (during which the spray is temporarily halted) using a 10 mm diameter flat-ended steel rod. The depth of erosion measured using the rod dictates the specimen erodability index: <20 mm after one hour is highly durable and >120 mm after one hour is a failure.

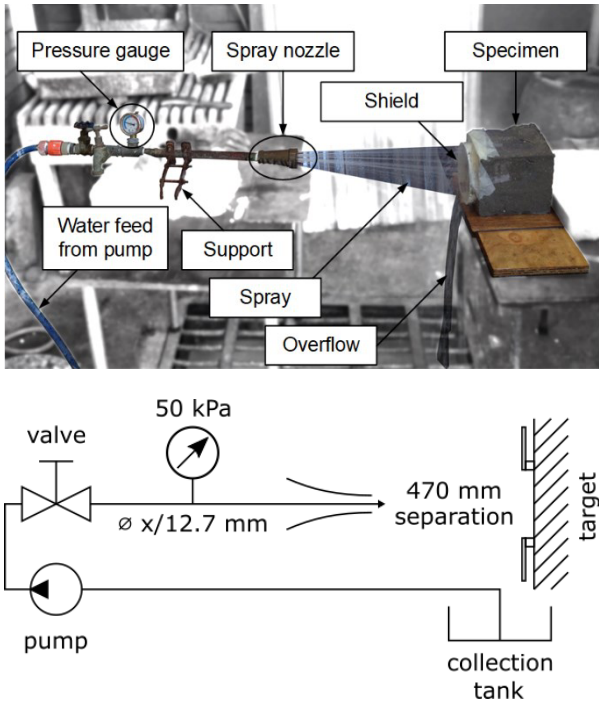

Fig. 1. CSIRO accelerated erosion test apparatus: top - annotated apparatus (photograph credit: Alessandro Arrigoni); bottom - hydraulic diagram where **x** is an unspecified external diameter.

2.2 Impact force

The underlying assumption of this work is that different tests can be compared according to the impact force of the spray on the specimen; for a given impact force, the specimen should erode at the same rate regardless of how that force is generated. The force of the spray impacting the specimen F (in N) is given by Equation 1, where Q is the volumetric flowrate (m^3/s), ρ_w is the density of water (kg/m^3), v_2 is the flow velocity on exiting the nozzle (m/s) and C_v is the dimensionless atmospheric deceleration coefficient ($C_v = 1$ for separation distances < 200 mm and $C_v = 1.1 - 0.5d$, where d is the separation distance in metres, thereafter).

$$F = \rho_w Q C_v v_2 \tag{1}$$

Given that the flow rate and velocity are not control parameters of the AET, it is useful instead to relate these to the delivery pressure and orifice cross sectional areas (Equations 2 and 3):

$$v_2 = \left(\frac{2(P_1 - P_2)}{\rho_w}\right)^{\frac{1}{2}} \tag{2}$$

$$Q = A_o v \tag{3}$$

where P_1 and P_2 (in Pa) are the pressure before and after the jet respectively and A_o is the cross-sectional area of the nozzle orifice (m^2, total cross section area if the orifice comprises multiple openings). $P_2 = 0$ if the spray discharges to the atmosphere.

As the nozzle obstructs the flow, it causes a drop in pressure. The pressure loss ΔP (in Pa) for incompressible flow through the nozzle specified in [6], where the total orifice area is greater than that of the upstream pipe and the orifice plate has a non-negligible thickness with respect to the orifice diameter, can be given by that across a thickened perforated plate (Equations 5-9):

$$f = {A_o}/{A_p} \tag{5}$$

$$k = \left[\frac{1}{2}(1-f)^{0.75} + \tau(1-f)^{1.375} + (1-f)^2 + \lambda\frac{l}{d_h}\right]\frac{1}{f^2} \tag{6}$$

$$\tau = \left(2.4 - \bar{l}\right)^{\phi(\bar{l})} \tag{7}$$

$$\phi(\bar{l}) = 0.25 + \left(\frac{0.535\bar{l}^8}{0.05 + \bar{l}^7}\right) \quad (8)$$

$$\Delta P = k\left(\frac{\rho_w v_p^2}{2}\right) \quad (9)$$

where f is the perforated plate "porosity" (dimensionless ratio of the open area of a plate segment to the total area of that segment), A_p (m^2) is the total area of the plate, $\bar{l} = \frac{l}{d_h}$ (dimensionless), l (m) is the thickness of the plate, d_h (m) is the hydraulic diameter, k (dimensionless) is the plate loss factor, and v_p is the flow velocity just prior to entering the perforated plate ($v_p = {Q}/{A_p}$, m/s). λ is a dimensionless parameter which varies with Reynolds number [12]. Under turbulent flow conditions, as are present in the AET, $k \approx 600$ with $l =$ 5 mm (average plate thickness in NZS 4297 [6]). Substituting Equations 2 to 9 into Equation 1 gives the theoretical impacting force considering a varying delivery pressure, nozzle geometry, and separation distance as defined by Equation 10.

$$F = 2C_v A_o(P_1 - \Delta P) \quad (10)$$

2.3 Apparatus

The apparatus used in this work to test variations in impact force with changes in the AET parameters is shown in Figures 2 and 3. The apparatus comprises a hinged plate which can swing freely against a load cell placed in line with the delivery pipe axis to measure the force. The load cell was selected for accuracy around loads of 1 N. A 600 mm×400 mm guard plate with a 150 mm diameter aperture is placed in front of the instrumented plate, again with the aperture in line with the delivery pipe axis. Both the guard plate and hinged panel are made from Perspex to allow the operator to see the water flow during testing. The delivery pipe is clamped to a central rail with multiple detents to allow for different separation distances to be tested easily. The apparatus sits above a collection tank, allowing the water to be recirculated as per Figure 1.

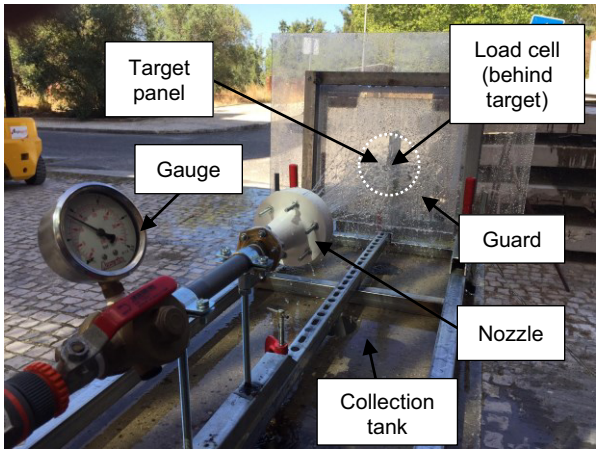

Fig. 2. Apparatus to test different configurations of accelerated erosion testing.

The nozzle specified by Middleton [4] is no longer in production. We therefore created a facsimile from polylactic acid (PLA) using 3D printing, following the work of Narloch et al. [13]. The final nozzle geometry is shown in Figure 4. The nozzle face comprises 35 orifices of 1.3 mm diameter, arranged in four rings about the central axis. Given the weaker PLA versus steel, the external geometry was modified to strengthen the nozzle walls and connection flanges whilst maintaining the internal geometry specified by NZS 4298 [6]. The nozzle face was printed separately to the body and bolted together, as seen in Figure 2, and a fixing plate was added to the rear of the nozzle in the place of the specified screw thread.

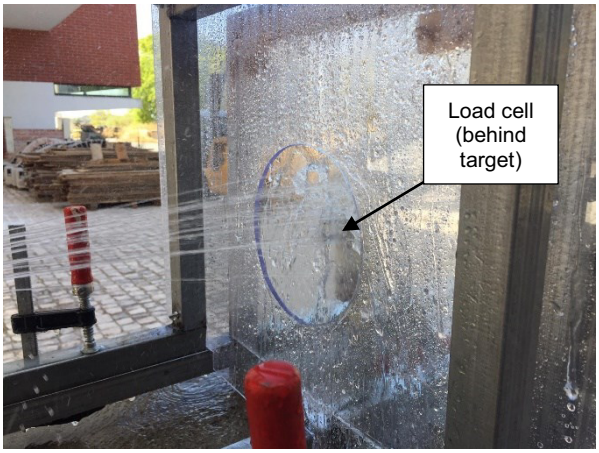

Fig. 3. View of the guard plate (150 mm diameter) in front of the instrumented target panel.

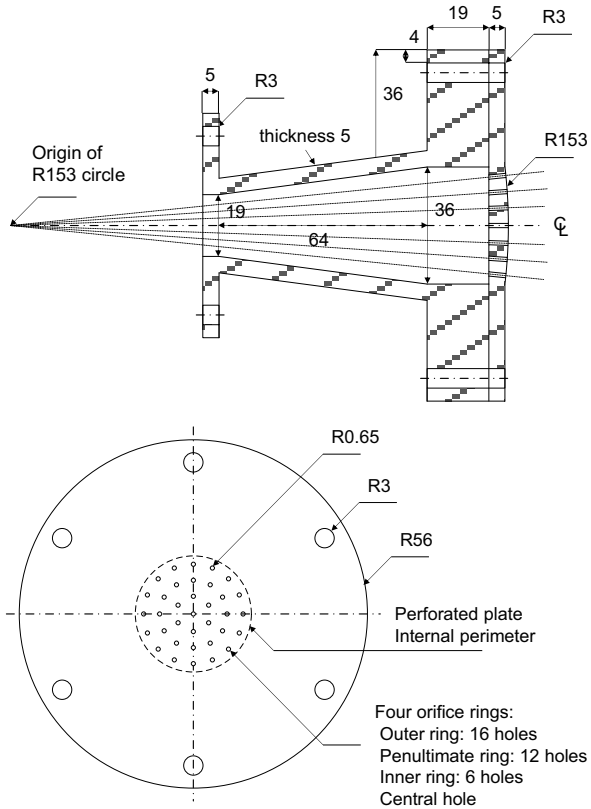

Fig. 4. Nozzle dimensions (in mm) adopted for 3D printing. All other dimensions as per NZS 4298 [6], Clause K.

2.4 Experimental programme

This study examined the effect of different delivery pressures and separation distances on the incident force as these variations are the most made common to the AET found in literature [9]. The nozzle geometry was kept constant for this work (as per Figure 4). We examined five separation distances (0.27 m, 0.37 m, **0.47 m**, 0.57 m, 0.67 m) and three delivery pressures (80 kPa, **50 kPa**, 20 kPa) to observe the effect of parameter changes either side of the AET specifications (NZS 4298 [6] specifications given in **bold text** in the above lists).

3 Results and discussion

The results from spray testing at different delivery pressures and distances are shown in Figure 5. For each test, the spray was delivered until reaching a steady state, whereupon the force was recorded and the spray halted.

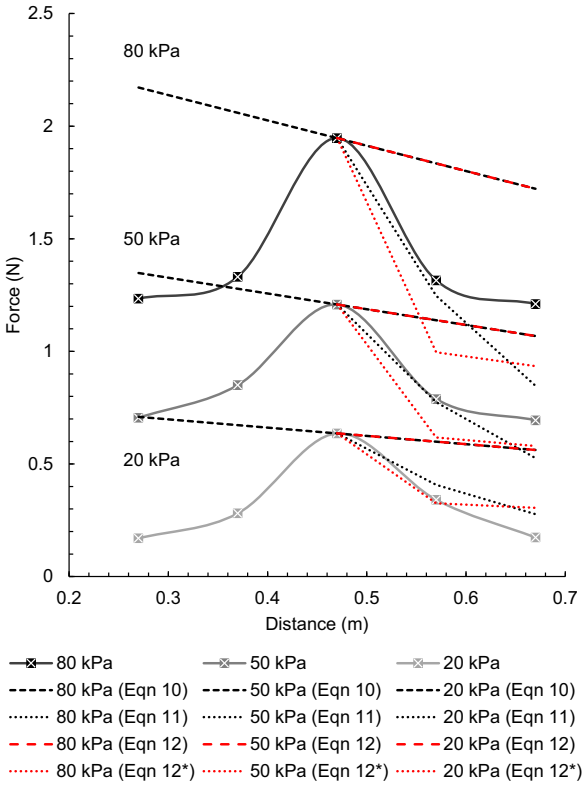

Fig. 5. Spray test results for measured and predicted impact forces with and without guard blocking for different delivery pressures and separation distances

For each delivery pressure, the measured force increased up to a separation distance of 470 mm and then decreased. This is contrary to the performance expected intuitively; we would believe that the force would be higher at shorter distances. However, at short separation distances, the water spray struck the target over a small area and was able to 'reverse'. The build-up of water blocked the incoming spray and reduced the incident steady-state force. At 470 mm, the spray was able to diverge sufficiently to cover the target area, which reduced fluid build-up and interference. Given the use of a smooth impermeable target instead of a textured permeable earthen sample, it is not obvious how much reversal would be expected for a real test. However, it is clear that reversal has a significant impact on the erosive force.

For this test, flow rate Q was not measured and so v_p and v_2 are unknown. Therefore, the measured force at a distance of 470 mm was used to estimate the pressure drop ΔP via Equation 10. The good match to measured values at 470 mm shown in Figure 5 using Equation 10 is therefore not necessarily indicative of a successful modelling process but is useful to compare the measured values to the predicted performance. It should be noted that this pressure drop is considerable: between 60 and 69% of the delivered pressure. This drop is due to the small orifice area of the plate compared to its total diameter (only 4.6% of the plate is open to flow). That such a pressure drop occurs in the nozzle supports the findings that the nozzle must be constructed robustly; our first 3D printed prototypes ruptured across the face when constructed to the dimensions given in NZS 4298 [6] Clause K, leading to the enlarged fixing plate shown around the nozzle face in Figure 4.

The force predicted using Equation 10 (black dashed lines in Figure 5) decreases with increasing separation distance due to the decreasing value of C_v: Q and A_o, and so ΔP, are constant for a given value of P_1. The poor match between Equation 10 and the forces recorded at short separation distances is expected, as flow reversal or interference is not considered in its derivation. However, the force decreased rapidly for separation distances above 470 mm, also contrary to Equation 10. This is because the spray cone diverged beyond the extent of the guard window, striking the guard as well as the target.

The loss in erosive force for distances over 470 mm can be investigated by considering the spray either to be a full cone or a collection of individual jets. If the spray has not diverged considerably then it can be considered to be a full cone (i.e. we can assume an even distribution of water across the cone cross section at the target distance). The real impact force F_i for a full cone which is partially intercepted by a guard is given by Equation 11, where $A_c = \pi(d \tan\theta)^2$ is the cross sectional area of the cone at the required separation distance, θ is the cone angle (the angle between the outer streamline and the spray axis), and A_t is the area of the target (here, a circle of 150 mm diameter). Equation 11 provides a good match to measured data for spray distances up to 570 mm, shown by the black dotted lines in Figure 5.

$$F_i = F \quad \text{for } d \le 470 \text{ mm}$$
$$F_i = \frac{A_t}{A_c} F \quad \text{for } d > 470 \text{ mm} \tag{11}$$

If the spray is able to diverge, then it can be treated as a collection of individual jets emanating from the nozzle face at the angles and in the pattern shown in Figure 4. The force on the target is then given by Equation 12, where a_s is the cross sectional area of one jet and $\sum a_s$ is the sum of all jet cross sections striking

the target area. For this calculation, A_o equals the sum of all jet cross sections originating from the nozzle.

$$F = \frac{\sum a_s}{A_o} F \tag{12}$$

Equation 12 is plotted in Figure 5, where it is assumed that i) jets are intercepted only if their incident angle would have them strike the guard plate (red dashed lines in Figure 5); and ii) that all jets emanating from the outer orifice ring are intercepted before striking the target for separation distances greater than 470 mm (red dotted lines in Figure 5 and denoted Equation 12*). The second case was considered as the spray was observed to become obstructed during testing for separation distances above 470 mm. Notably, this observation does not agree with the cone angle; for the orifice inclinations shown in Figure 4 and specified in NZS 4298 [6] Clause K, all jets should strike the target up to a distance of 750 mm (as shown by the red dashed line). That the outer jets were intercepted before that distance suggests that the orifice geometry was poorly controlled, perhaps due to the layer-wise deposition of 3D printing, or that the nozzle axis was not perfectly aligned to the delivery pipe or the target. Additionally, the effect of gravity on the streamwise direction is ignored and gravity may cause sufficient deflection for the jets to intercept the guard.

Equation 12* indicates that little change in the delivered force is expected between 570 mm and 670 mm, as only the outer jets are inhibited at both distances and the drop in force is governed by C_v only. This agrees well with the measured results for 80 kPa and 50 kPa, where little difference arose between those distances. However, Equation 12* increasingly underpredicts the measured force with increasing pressure (up to c.30% for a delivery pressure of 80 kPa), which indicates that some of the jets thought to be intercepted actually struck the target. Equations 11 and 12* therefore provide some reflection of reality but the effect of errors in nozzle and target geometry/manufacture and alignment remain significant if attempting to predict the impact force accurately.

It is worth commenting here that, under the Australian guidelines [11], a guard with a window of either 150 mm or 70 mm diameter can be placed in front of the specimen with no modification to the nozzle, pressure, or separation distance. This modification permits different materials to be tested; monolithic materials, for example rammed earth, can be built to be larger than 150 mm, whilst the smaller window allows for the testing of individual bricks (for example) that would otherwise not fill the window. From Equation 12, however, the force impacting the specimen is only approximately 54% for the 70 mm window at a separation distance of 470 mm, or only 21% by Equation 11. As discussed above, the real value is likely to be greater than the two but not equivalent to the force associated with the 150 mm diameter window. Under this modification, specimens tested using the smaller window would therefore score more highly than those using the larger.

4 Conclusion

This paper presented work started under Standards Australia committee BD 083 to provide guidance to compare variations to the New Zealand Standard accelerated erosion test which have arisen in literature and practice over the past few decades. By providing a comparison framework, the committee aimed to make the test more available, attractive, and relevant to earthen material practitioners and researchers.

The underlying assumption of this work is that different tests can be compared according to the impact force on the specimen delivered by the spray. In this paper, we examined the force delivered to a target during the NZS 4298 accelerated erosion test and how that force varied with changes in delivery pressure and separation distance. The impact force was measured using a hinged plate and load cell and the nozzle was fabricated to the key NZS 4298 Clause K dimensions using 3D printing. The measured force was compared to predictions from hydraulic theory, accounting for the pressure drop through the nozzle (here, modelled as flow through a thick perforated plate).

The results revealed several mechanisms that had not been considered in the theoretical modelling. At short separation distances (<470 mm), the flow impacting the target became trapped and reversed, interfering with the incoming flow and reducing the measured force. We note that replacing the earthen target with a smooth impermeable plate likely increased this effect however some degree of build-up would also be expected for an earthen target. At high separation distances (>470 mm), the spray struck the guard surrounding the target, reducing the amount of water reaching the target and so the overall force.

The general spray behaviour was well described by that of a full cone spray and a series of streamwise jets, transitioning between the two states as separation distance increased. Critically, however, this approach underpredicted measured values of the impact force by up to c.30% (for the range of conditions and assumptions tested) due to alignment errors in the delivery tube and nozzle geometry. Given the (purposefully) rudimentary construction of the AET apparatus, such errors are to be expected; however, their impact on the reliability of the theoretical framework is considerable.

Results presented here give confidence that the developed theoretical modelling can appraise the general variation in delivery force during an accelerated erosion test. As such, the modelling can provide a useful tool to compare the relative force delivered to a specimen during one accelerated erosion test to another. However, it is clear from the work completed so far that a generic framework cannot accurately capture the delivered force, perhaps by a significant magnitude. An attempt to create a framework for ‘generic’ accelerated erosion testing must, therefore, comprise a practical and a theoretical component to avoid poor material classification.

Acknowledgements

This work was supported by the University of Western Australia Faculty of Arts, Business, Law and Education through the School of Design research collaboration awards and contributes to the work of committee BD 083 Australian Earth Building. The second author would like to acknowledge the support of FCT for the partial funding of this work under the strategic project UIDB/04625/2020 from the research unit CERIS. The authors acknowledge feedback and support from the RILEM technical committees TC-274 and MAE.

References

1. Jaquin, P. A.; Augarde, C. E.; Gallipoli, D. & Toll, D. G. (2009). The strength of unstabilised rammed earth materials, Géotechnique, 59, 487-490
2. Beckett, C. T. S.; Augarde, C. E.; Easton, D. & Easton, T. (2018). Strength characterisation of soil-based construction materials, Géotechnique, 65, 400-409, DOI: 10.1680/jgeot.16.P.288
3. Minke, G. (2006). Building with earth --- Design and technology of a sustainable architecture, Birkhauser, Basel
4. Middleton, G. F. (1952). Bulletin 5: Earth-wall construction, CSIRO Division of Building, Construction and Engineering, North Ryde, Australia
5. NZS 4297:2020. Engineering design of earth buildings, Standards New Zealand
6. NZS 4298:2020. Materials and workmanship for earth buildings, Standards New Zealand
7. NZS 4299:2020. Earth buildings not requiring specific design, Standards New Zealand
8. ASTM (2010). ASTM E2392/E2392M-10 : Standard Guide for Design of Earthen Wall Building Systems, ASTM International, West Conshohocken, PA
9. Beckett, C. T. S.; Jaquin, P. A. & Morel, J.-C. (2020). Weathering the storm: A framework to assess the resistance of earthen structures to water damage, Construction and Building Materials, 242, 118098, DOI: 10.1016/j.conbuildmat.2020.118098
10. Heathcote, K. (1995). Durability of earthwall buildings, Construction and Building Materials, 9, 185-189
11. Walker, P. J. & Standards Australia (2002). HB 195: The Australian Earth Building Handbook, SAI Global Ltd., Sydney, Australia
12. Idelchik, I. E. Ginevskiy, A. S. & Kolesnikov, A. V. (Eds.) (2007). Handbook of hydraulic resistance, Begell House, Inc., 50 Cross Highway, Redding, CT 06896
13. Narloch, P. L.; Woyciechowski, P.; Dmowska, E. & Halemba, K. (2015). Durability assessment of monolithic rammed earth walls, Archives of Civil Engineering, 61, 73-88, DOI: 10.1515/ace-2015-0015